CHEMICAL SENSING

Aptamer–field-effect transistors overcome Debye length limitations for small-molecule sensing

Nako Nakatsuka[1,2], Kyung-Ae Yang[3], John M. Abendroth[1,2], Kevin M. Cheung[1,2], Xiaobin Xu[1,2], Hongyan Yang[4], Chuanzhen Zhao[1,2], Bowen Zhu[1,5], You Seung Rim[1,5]*, Yang Yang[1,5], Paul S. Weiss[1,2,5]†, Milan N. Stojanović[3,6]†, Anne M. Andrews[1,2,4]†

Detection of analytes by means of field-effect transistors bearing ligand-specific receptors is fundamentally limited by the shielding created by the electrical double layer (the "Debye length" limitation). We detected small molecules under physiological high–ionic strength conditions by modifying printed ultrathin metal-oxide field-effect transistor arrays with deoxyribonucleotide aptamers selected to bind their targets adaptively. Target-induced conformational changes of negatively charged aptamer phosphodiester backbones in close proximity to semiconductor channels gated conductance in physiological buffers, resulting in highly sensitive detection. Sensing of charged and electroneutral targets (serotonin, dopamine, glucose, and sphingosine-1-phosphate) was enabled by specifically isolated aptameric stem-loop receptors.

Field-effect transistors (FETs) modified with target-specific receptors could enable direct electronic target detection (*1*, *2*). Signal transduction and amplification in FET-based sensors is based on electrostatic gating of thin-film semiconductor channels by target-receptor interactions, such that even low receptor occupancy measurably affects transconductance (*3*). However, receptor-modified FETs must overcome two fundamental limitations to become more widely adopted: (i) In solutions containing ions, the electrical double layer shields semiconductor charge carriers to limit gating in response to recognition events. The extent of shielding (i.e., the effective sensing distance) is characterized by the Debye length, which in physiological fluids is <1 nm (table S1) (*4*). (ii) Small target molecules with few or no charges have minimal impact on semiconductor transconductance unless they trigger conformational changes in charged receptors within or near the Debye length, or otherwise affect surface potentials (*5*).

We overcame both of these obstacles by combining highly sensitive FETs with a specific type of oligonucleotide stem-loop receptor selected for adaptive target recognition (Fig. 1A). We fabricated nanometer-thin In_2O_3 FETs (Fig. 1B) using methods that facilitate micro- and nanoscale patterning and are readily scalable for producing large numbers of devices (*2*, *6*). Sensing with FETs is inherently nonlinear (*5*), which enables target detection over larger and lower concentration ranges than can be achieved with equilibrium-based sensors (*7*). Although aptamers have been used as receptors for FET devices (*2*, *8*), it proved critical to combine ligand-induced stem-loop conformational rearrangements and close proximity to the surfaces of quasi–two-dimensional FETs. Changes in conformation of negatively charged phosphodiester backbones enabled signal transduction and amplification under biologically relevant conditions with low-charge and neutral targets.

Solution-phase selection of aptamers circumvented tethering of small-molecule targets and was based on stem-loop closing with appropriate counterselection against interferents (Fig. 1C) (*9*, *10*). This approach yielded aptamers characterized by adaptive-loop binding. Strategies and details of the selections and counterselections are given in fig. S1 and tables S2 and S3. We isolated original receptors for dopamine, serotonin, glucose, and sphingosine-1-phosphate (S1P) (Fig. 1, D to G, and table S4). Dopamine was targeted because we had constructed FET devices using a previously reported dopamine aptamer (*11*), but these required dilute ion concentrations for sensing (*2*). Serotonin was pursued as another important neurotransmitter target (*12*) having no reported aptamer sequences. Ultimately, we aim to distinguish serotonin from dopamine and other similarly structured molecules in measurements of interneuronal signaling (*13*–*15*). Glucose was selected as an example of an important neutral target. Aptamers interacting directly with glucose have not been reported (although compare with aptamers for glucose sensors) (*10*). The lipid S1P (critical micellar concentration <10 μM), which prevents chemotherapy-associated apoptosis (*16*), was chosen as an example of a zwitterionic target.

Fluorescence assays were used to characterize aptamer-target dissociation constants (K_d) (fig. S2A). Selection led to high-affinity aptamers for dopamine (150 nM) and serotonin (30 nM) (fig. S2, B and C). Counterselection minimized interactions with other neurotransmitters and metabolites (Fig. 1, H and I) critical for sensing in the presence of high concentrations of similarly structured countertargets in vivo. Notably, our dopamine aptamer did not recognize norepinephrine, in contrast to cross-reactivity of a previously reported dopamine aptamer (*2*, *11*). Poor selectivity has also been problematic for fast-scan cyclic voltammetry, the most common method for sensing dopamine (*13*, *17*). The affinity of the glucose aptamer (~10 mM) (fig. S2D) and selectivity with respect to analogs (Fig. 1J and fig. S3) were consistent with the receptor recognizing hydrophobic surfaces of glucose (*18*). The affinity of the S1P aptamer was 180 nM (Fig. 1K and fig. S2E), which was not as high as a reported mirror-image aptamer (4 nM) (*19*).

We covalently modified thin-film In_2O_3 FETs with dopamine or serotonin aptamers using silane chemistry (fig. S4) to investigate electronic small-molecule detection (Fig. 1A). Despite subnanometer Debye screening lengths, aptamer-FETs responded to wide ranges of target concentrations (10^{-14} to 10^{-9} M) in undiluted (i.e., physiological) phosphate-buffered saline (1× PBS; Fig. 2A and fig. S5A) or artificial cerebrospinal fluid (aCSF; Fig. 2, B and C) with response times on the order of seconds (fig. S6). Scrambled aptamer sequences (table S5) produced negligible responses (Fig. 2, A to C, and fig. S5A), as did FETs lacking aptamers (fig. S5, B and C). Even at physiological ion concentrations (and hence substantially reduced Debye lengths), FET responses for our dopamine aptamer were more than three orders of magnitude greater than those of the previously reported dopamine aptamer (*11*) in 0.1× PBS (Fig. 2A) because of the designed positioning of recognition regions capable of adaptive conformational changes in the new aptamer.

Dopamine aptamer–FETs were selective for dopamine versus serotonin, norepinephrine, tyramine, and dopamine metabolites (Fig. 2D and fig. S7A). Serotonin aptamer–FETs were selective for serotonin versus dopamine, norepinephrine, histamine, other biogenic amines, and indole metabolites (Fig. 2E and fig. S7B). Aptamer-FET selectivity was further investigated with surface-enhanced Raman spectroscopy (SERS; fig. S8, A and B). Raman signatures were enhanced only in close proximity to metal surfaces because of the short range of evanescent fields, with the strongest enhancement within ~1 nm of surfaces (similar to the physiological Debye length) (*20*). After dopamine or serotonin were introduced, SERS spectra exhibited complex pattern changes that were not evident with nontarget compounds (fig. S8, C and D).

Concentration sensitivity ranges could be "tuned" by altering the numbers of serotonin aptamers on FET surfaces (Fig. 2F). To evaluate sensing in an undiluted biological matrix, we

[1]California NanoSystems Institute, University of California, Los Angeles, CA 90095, USA. [2]Department of Chemistry and Biochemistry, University of California, Los Angeles, CA 90095, USA. [3]Center for Innovative Diagnostic and Therapeutic Approaches, Department of Medicine, Columbia University, New York, NY 10032, USA. [4]Department of Psychiatry and Biobehavioral Science, Semel Institute for Neuroscience and Human Behavior, and Hatos Center for Neuropharmacology, University of California, Los Angeles, CA 90095, USA. [5]Department of Materials Science and Engineering, University of California, Los Angeles, CA 90095, USA. [6]Departments of Biomedical Engineering and Systems Biology, Columbia University, New York, NY 10032, USA.
*Present address: School of Intelligent Mechatronics Engineering, Sejong University, Seoul 05006, Republic of Korea.
†Corresponding author. Email: aandrews@mednet.ucla.edu (A.M.A.); mns18@cumc.columbia.edu (M.N.S.); psw@cnsi.ucla.edu (P.S.W.)

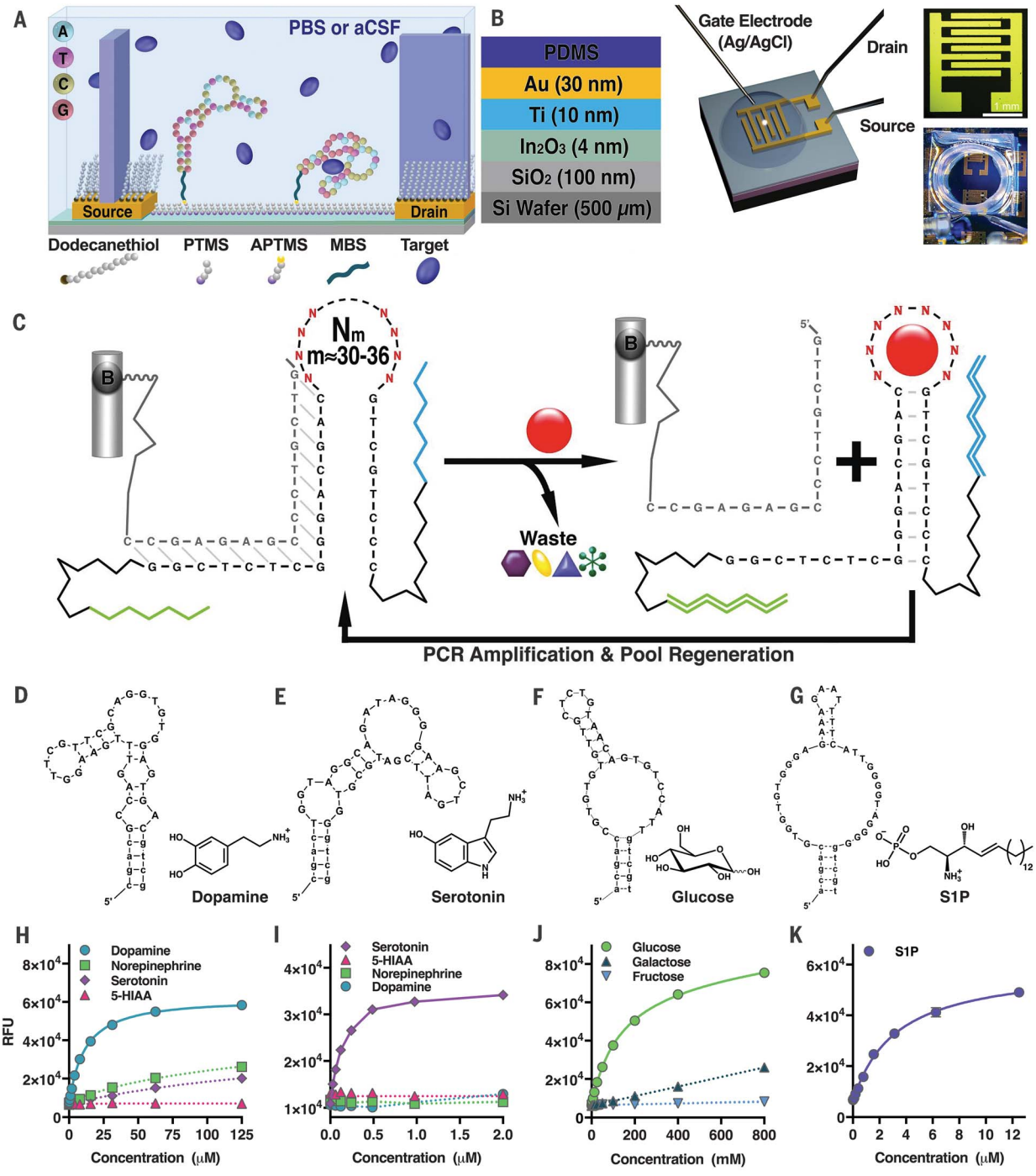

Fig. 1. Isolation of stem-loop aptamer receptors. (**A**) Schematic of FET surface chemistry. PTMS, trimethoxy(propyl)silane; APTMS, (3-aminopropyl)trimethoxysilane; MBS, 3-maleimidobenzoic acid *N*-hydroxysuccinimide ester. (**B**) Layer-by-layer composition of FETs, FET microscope image, and photograph of experimental setup. PDMS, polydimethylsiloxane. (**C**) Oligonucleotide libraries (N_m, with random regions m from 30 to 36 nucleotides, flanked by constant regions and oligonucleotide primer regions for polymerase chain reaction amplification) were attached to agarose-streptavidin columns via biotinylated (B) complementary sequences. Exposure to targets (red sphere) causes elution of aptamers in which stems are stabilized. These sequences are preferentially amplified. Exposure to countertargets (alternative shapes) eliminates cross-reactive sequences. (**D** to **K**) Aptamers for dopamine (K_d = 150 nM) (D), serotonin (K_d = 30 nM) (E), glucose (K_d = 10 mM) (F), and S1P (K_d = 180 nM) (G) were isolated. Solution-phase SELEX (i.e., systematic evolution of ligands by exponential enrichment) was used to identify aptamers that were directly converted to sensors. The complementary oligonucleotide was labeled with a quencher instead of biotin, whereas the aptamer was labeled with a fluorophore (table S4), leading to adaptive binding sensors with responses shown in (H) to (K). Fluorescence responses indicate selectivities of dopamine, serotonin, and glucose aptamers in the presence of specific versus nonspecific targets. Fluorescence-concentration curves (RFU, relative fluorescence units) were the result of *N* = 3 measurements with SEMs too small to be visualized in the graphs shown.

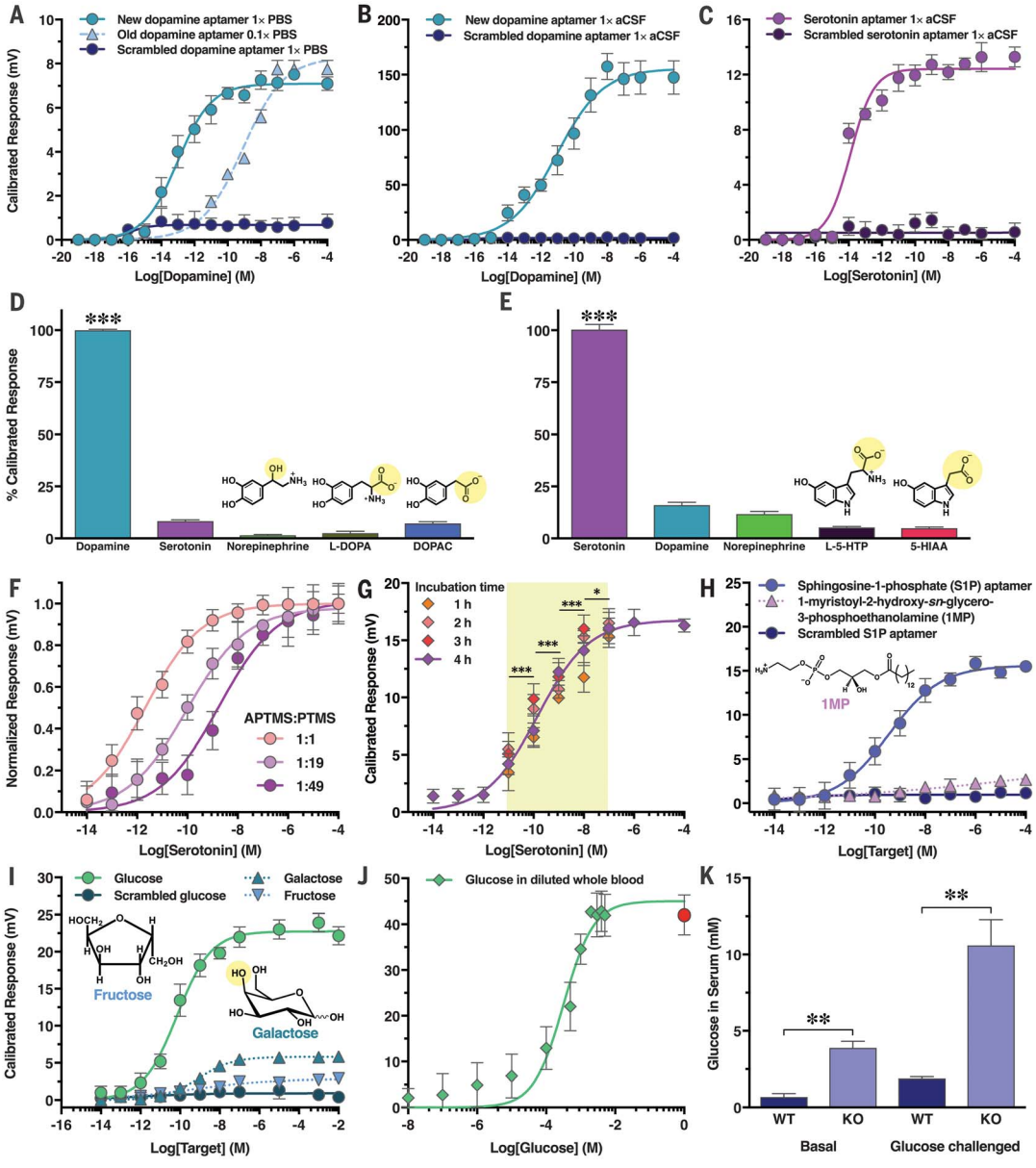

Fig. 2. Electronic small-molecule detection using aptamer-functionalized FET sensors. (**A**) Responses of FET sensors functionalized with the new dopamine aptamer [K_d = 150 nM, full-strength PBS (1× PBS)] or its scrambled sequence, compared to FET responses with a previously reported dopamine aptamer (K_d = 1 μM, 0.1× PBS) (*2*). (**B**) New and scrambled dopamine aptamer–FET responses to dopamine in 1× aCSF. (**C**) For serotonin aptamer–FETs, serotonin in 1× aCSF led to concentration-dependent responses, whereas scrambled serotonin sequences showed negligible responses. (**D**) New dopamine aptamer–FET responses to 100 μM norepinephrine, serotonin, L-3,4-dihydroxyphenylalanine (L-DOPA), and 3,4-dihydroxyphenylacetic acid (DOPAC) were negligible relative to dopamine (10 nM). (**E**) Serotonin aptamer–FET responses to 100 μM dopamine, norepinephrine, L-5-hydroxytryptophan (L-5-HTP), or 5-hydroxyindoleacetic acid (5-HIAA) were negligible relative to serotonin (10 nM). (**F**) Serotonin aptamer–FET sensitivities were shifted by altering ratios of amine-terminated/methyl-terminated silanes for surface tethering. (**G**) Serotonin aptamer–FETs after 1 to 4 hours of incubation in serotonin-free brain tissue followed by addition of serotonin exhibited reproducible responses with differentiable physiological concentrations. (**H**) S1P aptamer–FETs showed concentration-dependent responses to S1P but not to a phospholipid with similar epitopes or a scrambled sequence in 1× HEPES. (**I**) Glucose sensing in 1× Ringer's buffer. Responses of glucose aptamer–FETs were minimal or negligible for galactose, fructose, and a scrambled sequence. (**J**) Glucose aptamer–FET responses in mouse whole blood diluted in Ringer's to construct a concentration curve. The red circle represents response in undiluted whole blood. (**K**) Glucose aptamer–FETs enabled differentiation of hyperglycemia in serotonin transporter–deficient (KO) mice versus wild-type (WT) mice by measuring glucose levels in diluted serum under basal and glucose-challenged conditions. All calibrated responses were at gate voltage V_G = 100 mV. Error bars are ± SEM with N = 6 [(A) to (C), (H), (I), and (K)] or N = 3 samples per group [(D) to (G) and (J)]. In (D) and (E), ***P < 0.001 versus countertargets; in (G), ***P < 0.001, *P < 0.05 versus different serotonin concentrations (10 pM to 100 nM); in (K), **P < 0.01 KO versus WT. **P < 0.01 KO versus WT.

added serotonin to brain tissue from mice lacking neuronal serotonin (i.e., *Tph2* null mice) (Fig. 2G) (*21*). Electronic FET responses differentiated physiologically relevant serotonin concentrations (10 pM to 100 nM) (*14*). Sensor responses to dopamine or to the serotonin metabolite 5-hydroxyindoleacetic acid in tissue were negligible (fig. S9A). The high sensitivity of aptamer-FETs offsets losses often encountered in biological environments, and sensitivity for modest changes in target concentrations was observed despite large sensing ranges. Sensor performance in tissue was reproducible when repeated 12 hours later (fig. S9B). Moreover, continuous exposure of serotonin aptamer–FETs to brain tissue for 1 to 4 hours produced stable concentration-dependent conductance responses and was another indication of sensor stability (Fig. 2G).

Aptamer-FET responses to the zwitterionic lipid S1P were recorded at concentrations ranging from 10 pM to 100 nM. A nontarget lipid (1-myristoyl-2-hydroxy-*sn*-glycero-3-phosphoethanolamine) bearing similar epitopes (Fig. 2H) exhibited negligible responses, as did a scrambled S1P sequence (table S5). Glucose aptamer–FETs exhibited concentration-dependent responses to glucose (10 pM to 10 nM). The FET responses to other monosaccharides (e.g., galactose and fructose) were minimal, as were responses when a scrambled glucose sequence was used (Fig. 2I and table S5). Experiments with SERS corroborated target-specific recognition in close proximity to substrates for S1P and glucose aptamers (fig. S8, E and F).

We detected glucose in whole blood diluted with Ringer's buffer (10 μM to 1 mM; Fig. 2J). We also measured glucose levels in diluted serum from mice lacking serotonin transporter expression characterized by hyperglycemia (*22*). Elevations in serum glucose in basal and glucose-challenged states were observed using glucose aptamer–FETs (Fig. 2K); glucose concentrations were similar to those determined in whole blood using a glucometer (fig. S10). These findings demonstrated the feasibility of aptamer-FET sensing in diluted, yet full–ionic strength, blood or serum and the ability to differentiate modest yet physiologically relevant differences in neutral target concentrations.

Aptamer-FET sensing enabled observations suggestive of mechanism. In addition to FET responses at subthreshold-regime gate voltages (Fig. 2), we examined characteristics of FET transfer curves [i.e., source-drain currents (I_{DS}) versus source-gate voltage sweeps (V_{GS})]. Transfer curves for increasing target concentrations diverged for dopamine aptamer– and glucose aptamer–FETs versus serotonin aptamer– and S1P aptamer–FETs (Fig. 3, A to D). Dopamine and serotonin each have one positive charge at physiological pH. Transfer curve divergence for these molecules enables us to conclude that signal transduction mechanisms based exclusively on target charge, as has been proposed (*23*), are incorrect and preclude detection of neutral targets. The divergence of *I-V* curves also suggests different conformational changes upon target binding. For dopamine and glucose, transfer curves were consistent with aptamer reorientations occurring such that substantial portions of the negatively charged backbones moved closer to n-type semiconductor channels, thereby increasing electrostatic repulsion of charge carriers (band bending) and decreasing transconductance, measured as target-related current responses (Fig. 3E). In contrast, we hypothesized that serotonin and S1P aptamers moved predominantly away from channel surfaces upon target capture, thereby increasing transconductance (Fig. 3F).

We used circular dichroism (CD) spectroscopy to gain additional insight (*24*, *25*). For dopamine and serotonin, large changes in CD peak positions and relative intensities suggested shifts away from predominant duplex signals (maxima at ~280 nm) and formation of new target-induced structural motifs. A parallel (or mixed) G-quadruplex (maximum shifted to 260 nm) (*26*) was suggested for dopamine-aptamer complexes (Fig. 4A), whereas an antiparallel G-quadruplex (maximum shifted to 290 nm) was indicated for serotonin-aptamer

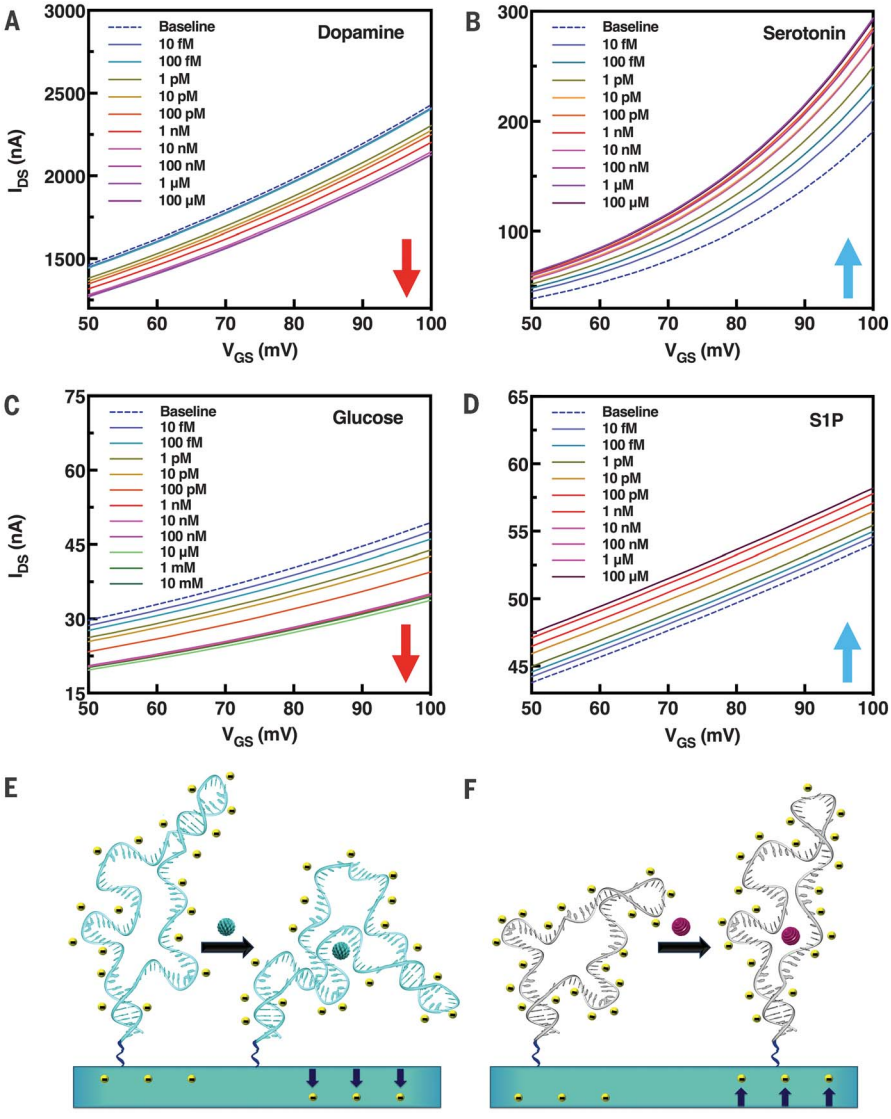

Fig. 3. Aptamer-functionalized FET mechanisms. (**A**) Exposure of dopamine aptamer–FETs to dopamine (1× aCSF) led to concentration-dependent reductions in source-drain currents. (**B**) For serotonin aptamer–FETs, increasing concentrations of serotonin (1× aCSF) produced increases in source-drain currents. (**C**) Exposure of glucose aptamer–FETs to glucose (1× Ringer's) led to reductions in source-drain currents. (**D**) The S1P aptamer–FET transfer curves (1× HEPES) increased in response to target concentrations. Transfer curves shown are representative of $N = 6$ individual measurements. (**E** and **F**) Hypothesized mechanism of stem-loop aptamer target-induced reorientations in close proximity to semiconductor channels and within or near the Debye length. In (E), aptamers reorient closer to FETs to deplete channels electrostatically (e.g., dopamine, glucose). In (F), aptamer stem-loops reorient away from semiconductor channels, thereby increasing transconductance (e.g., serotonin, S1P). Schematics are idealized and do not reflect individual aptamer secondary structural motifs.

complexes (Fig. 4B). As with fluorescence, FET, and SERS data, CD indicated selectivity of dopamine and serotonin aptamers for their targets versus similarly structured countertargets (fig. S11, A and B). Although fluorescence, FET, and SERS findings specified target recognition for glucose and S1P aptamers, changes in CD spectra were not observed for these aptamers (fig. S11, C and D). Thus, for glucose and S1P aptamers, all major DNA domains (i.e., G-quartets, helices, and single-stranded regions) were formed prior to target binding, and adaptive binding occurred through spatial rearrangement of existing secondary structures and companion ions (*27*).

We used Förster resonance energy transfer (FRET) to investigate changes in aptamer backbone distances during target-induced conformational changes. We identified FRET sensors for serotonin and glucose aptamers (table S6). For serotonin, the decrease in FRET (Fig. 4C and fig. S12A) was consistent with a substantial fraction of the longest loop in the G-quadruplex moving away from the semiconductor surface, and hence with the upward shifts in FET transfer curves (Fig. 3B). For glucose, FRET results (Fig. 4D and fig. S12B) supported movement of the second stem in the aptamer toward the semiconductor surface, consistent with downward shifts in FET transfer curves (Fig. 3C). For the glucose aptamer, we increased the stem lengths for attachment to FET surfaces (Fig. 4E). Conductance responses decreased with additional base pairs (Fig. 4F), which suggested that recognition occurred farther away from FETs as the attachment stems became longer. This strategy might be used to tune sensitivity ranges of sensor array elements, thereby extending the ranges of arrays.

Together, all mechanistic findings are consistent with aptamer conformational changes enabling FET sensing under physiological conditions and without aptamer labeling or additional surface chemistries [compare with (*28*)]. Note that because of the aptamer selection strategy, target-specific aptamer reorientations occur in close proximity to semiconductor surfaces, and in some cases, even in the absence of formation of new secondary structural motifs. General aptamer reorientation can be inferred from FET gate-voltage sweeps, with additional FET mechanisms possibly contributing for specific sensors (e.g., band bending) and permittivity and mobility changes. Unlike large protein receptors (e.g., antibodies), highly selective, chemically synthesized, compact nucleic acid receptors identified through in vitro selection are amenable to affinity tuning (*29*, *30*) and targeting of a wide variety of small (and large) molecules for electronic sensing (*23*).

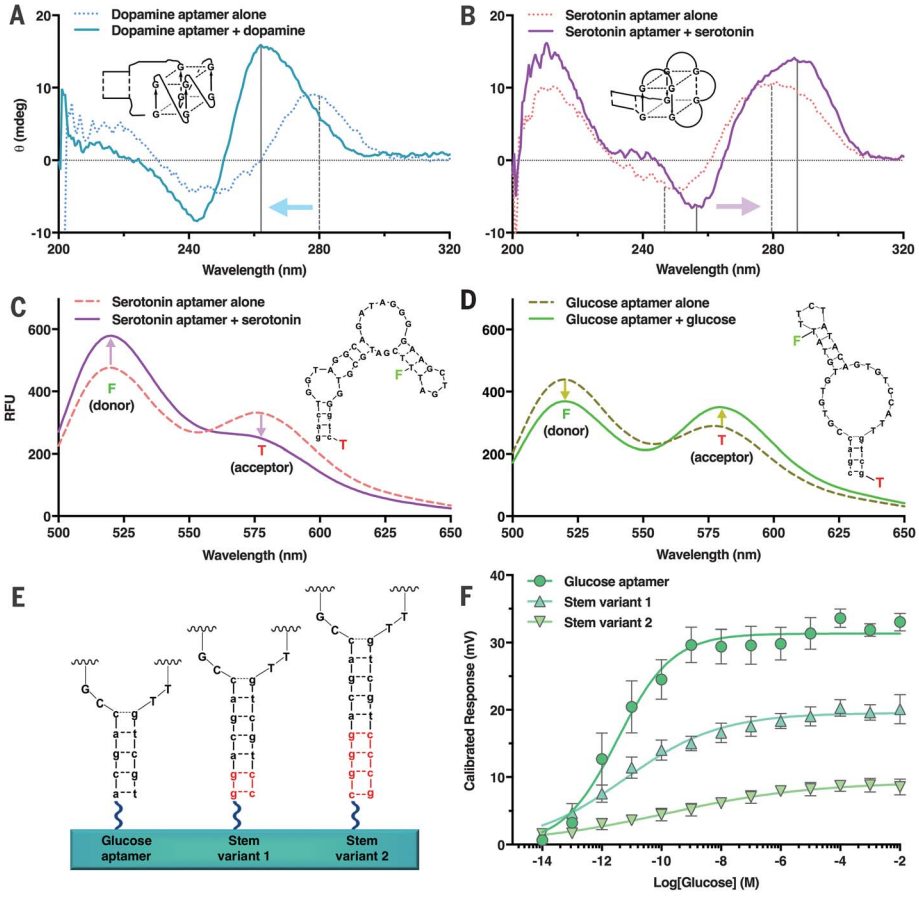

Fig. 4. Changes in aptamer secondary structures upon adaptive binding to small-molecule targets. (**A**) Circular dichroism spectroscopy of the dopamine aptamer upon target capture showed spectral shifts indicating formation of a parallel G-quadruplex (1× aCSF). (**B**) By contrast, the serotonin aptamer showed shifts in peak positions indicating formation of an antiparallel G-quadruplex. (**C** and **D**) FRET between donor- [fluorescein (F), excited at 470 nm] and acceptor-[5-carboxytetramethylrhodamine (T)] labeled aptamers was monitored before and after target incubation. For serotonin aptamers (C), donor fluorescence increased while acceptor emission decreased upon serotonin incubation, suggesting that fluorophores move farther away from each other upon target exposure. Conversely, for glucose aptamers (D), the emission spectra for the acceptor increased while donor fluorescence decreased upon glucose exposure, indicative of the acceptor moving closer to the donor, thereby enabling increased energy transfer. Stem-loop movement directions indicated by FRET for glucose versus serotonin aptamers are consistent with their divergent FET transfer curve directions in Fig. 3. (**E** and **F**) For glucose aptamer–FETs with rigid double-stranded attachment stems [(E), left], increasing distances from semiconductor surfaces by increasing the stem lengths [(E), stem variants, right] resulted in length-associated decreases in FET calibrated responses (1× Ringer's solution) (F). Spectra shown in (A) to (D) are representative of $N = 2$ samples per condition; error bars in (F) are ±SEM with $N = 3$ samples per group.

REFERENCES AND NOTES

1. Y. Cui, Q. Wei, H. Park, C. M. Lieber, *Science* **293**, 1289–1292 (2001).
2. J. Kim *et al.*, *ACS Nano* **9**, 4572–4582 (2015).
3. P. Casal *et al.*, *Philos. Trans. R. Soc. A* **370**, 2474–2488 (2012).
4. A. Vacic *et al.*, *J. Am. Chem. Soc.* **133**, 13886–13889 (2011).
5. P. S. Weiss, P. L. Trevor, M. J. Cardillo, *J. Chem. Phys.* **90**, 5146–5153 (1989).
6. W. S. Liao *et al.*, *Science* **337**, 1517–1521 (2012).
7. K. Shoorideh, C. O. Chui, *Proc. Natl. Acad. Sci. U.S.A.* **111**, 5111–5116 (2014).
8. M. P. Landry *et al.*, *Nat. Nanotechnol.* **12**, 368–377 (2017).
9. R. Nutiu, Y. Li, *Angew. Chem. Int. Ed.* **44**, 1061–1065 (2005).
10. K. A. Yang *et al.*, *Nat. Chem.* **6**, 1003–1008 (2014).
11. R. Walsh, M. C. DeRosa, *Biochem. Biophys. Res. Commun.* **388**, 732–735 (2009).
12. S. C. Altieri *et al.*, *Neuropsychopharmacology* **40**, 1456–1470 (2015).
13. N. Nakatsuka, A. M. Andrews, *ACS Chem. Neurosci.* **8**, 218–220 (2017).
14. H. Yang, A. B. Thompson, B. J. McIntosh, S. C. Altieri, A. M. Andrews, *ACS Chem. Neurosci.* **4**, 790–798 (2013).
15. A. P. Alivisatos *et al.*, *ACS Nano* **7**, 1850–1866 (2013).
16. G. I. Perez, C. M. Knudson, L. Leykin, S. J. Korsmeyer, J. L. Tilly, *Nat. Med.* **3**, 1228–1232 (1997).
17. N. T. Rodeberg, S. G. Sandberg, J. A. Johnson, P. E. M. Phillips, R. M. Wightman, *ACS Chem. Neurosci.* **8**, 221–234 (2017).
18. C. Ke, H. Destecroix, M. P. Crump, A. P. Davis, *Nat. Chem.* **4**, 718–723 (2012).
19. W. G. Purschke *et al.*, *Biochem. J.* **462**, 153–162 (2014).
20. S. S. Masango *et al.*, *Nano Lett.* **16**, 4251–4259 (2016).
21. M. Angoa-Pérez *et al.*, *ACS Chem. Neurosci.* **5**, 908–919 (2014).
22. X. Chen, K. J. Margolis, M. D. Gershon, G. J. Schwartz, J. Y. Sze, *PLOS ONE* **7**, e32511 (2012).
23. N. Nakatsuka, P. S. Weiss, A. M. Andrews, *Chem. Rev.* (2018).
24. W. Liu *et al.*, *J. Phys. Chem. B* **115**, 13051–13056 (2011).
25. S. Nagatoishi, Y. Tanaka, K. Tsumoto, *Biochem. Biophys. Res. Commun.* **352**, 812–817 (2007).
26. J. Kypr, I. Kejnovská, D. Renčiuk, M. Vorlíková, *Nucleic Acids Res.* **37**, 1713–1725 (2009).
27. Y. Nagai *et al.*, *Langmuir* **29**, 9951–9957 (2013).
28. N. Gao *et al.*, *Proc. Natl. Acad. Sci. U.S.A.* **113**, 14633–14638 (2016).
29. F. Ricci, A. Vallée-Bélisle, A. J. Simon, A. Porchetta, K. W. Plaxco, *Acc. Chem. Res.* **49**, 1884–1892 (2016).
30. R. E. Armstrong, G. F. Strouse, *Bioconjug. Chem.* **25**, 1769–1776 (2014).

ACKNOWLEDGMENTS

We thank D. Kuhn and H. Chen for resources and assistance, and K. Gothelf for helpful discussion. **Funding:** Supported by NIH (DA045550, CA199849, GM104960), NSF (CCF1518715, 1509794, CMMI-1636136), CalBrain, NantWorks, Hewlett Packard, the Merkin Family Foundation, and the China Scholarship Council. **Author contributions:** N.N., K.A.Y., P.S.W., M.N.S., and A.M.A. conceived experiments; N.N. and K.M.C. performed aptamer-FET measurements; K.A.Y. and M.N.S. designed and isolated stem-loop aptamer receptors and conducted FRET measurements; N.N., J.M.A., and X.X. conducted spectroscopy experiments; H.Y. carried out mouse experiments; C.Z., B.Z., Y.S.R., and Y.Y. designed and fabricated thin-film transistors; and N.N., P.S.W., M.N.S., and A.M.A. wrote the manuscript. **Competing interests:** N.N., K.A.Y., P.S.W., M.N.S., and A.M.A. have filed a patent on stem-loop receptor-based field effect sensor devices for sensing at physiological salt concentrations, U.S. application no. 504901225. M.N.S. has patent applications, a start-up company, and consulting income for work on small-molecule aptamers. **Data and materials availability:** All data needed to evaluate the conclusions in the paper are presented in the paper or the supplementary materials.

SUPPLEMENTARY MATERIALS

www.sciencemag.org/content/362/6412/319/suppl/DC1
Materials and Methods
Figs. S1 to S17
Tables S1 to S9
References (*31*–*55*)

15 August 2017; resubmitted 30 April 2018
Accepted 6 August 2018
Published online 6 September 2018
10.1126/science.aao6750